

**SURFACE OXIDATION OF CU EXTRACTED
FROM ELECTRONIC WASTE FOR CUO
NANOWIRES FORMATION AND THEIR USE TO
REDUCE CR(VI)**

YONG HUI SIN

UNIVERSITI SAINS MALAYSIA

2022

**SCHOOL OF MATERIALS AND MINERAL RESOURCES ENGINEERING
UNIVERSITI SAINS MALAYSIA**

**SURFACE OXIDATION OF CU EXTRACTED FROM ELECTRONIC WASTE
FOR CUO NANOWIRES FORMATION AND THEIR USE TO REDUCE CR(VI)**

By

YONG HUI SIN

Supervisor: Professor Dr. Zainovia Lockman

Dissertation submitted in partial fulfillment of the requirements for the degree of

Bachelor of Engineering with Honours

(Materials Engineering)

Universiti Sains Malaysia

August 2022

DECLARATION

I hereby declare that I have conducted, completed the research work and written the dissertation entitled “Surface oxidation of Cu extracted from electronic waste for CuO nanowires formation and their use to reduce Cr(VI)”. I also declare that it has not been previously submitted for the award of any degree or diploma or other similar title of this for any other examining body or University.

Name of Student: Yong Hui Sin

Date: 12/08/2022

Signature:



Witness by

Supervisor: Prof. Dr. Zainovia Lockman

Date: 12/08/2022

Signature:



ACKNOWLEDGEMENT

First and foremost, I would like to express my utmost gratitude to my supervisor, Professor Dr. Zainovia Lockman for patiently guiding and supporting me throughout the completion of the Final Year Project. This project would not be a success without her professional advice and guidance. With her years of experience as a lecturer and researcher, she had imparted the essential experimental skills, techniques and knowledge to me in order for me to complete this project.

Furthermore, I also would like to thank to the technical staffs involved, Mr Azam, Mr Azrul, Mr Junaidi and Mr Saarani for helping me a lot during conducting the experiment in this research. I really appreciate all of the advice and opinion that have being given to me. Special thanks to Dr. Suhaina for providing insights on the recovery of copper from waste printed circuit board. Apart from that, special acknowledgement is to be given to Prof Ir. Ts. Dr. Anasyida Bt Abu Seman. She has given the guideline for the entire final year students and arranged sessions to teach us generally regarding the writing skill and the correct technique to have proper thesis writing.

I would also like to thanks to Prof. Dr. Zainovia's research team for all the assistance and guidance provided to me throughout the entire project. This project would not be able to complete without their patient guidance and support to me.

Last but not least, I also would like to thank to my family and friends for being supportive and motivate me in competing this project.

TABLE OF CONTENTS

	Page
ACKNOWLEDGEMENT	iii
TABLE OF CONTENTS	iv
LIST OF TABLES	vii
LIST OF FIGURES	viii
LIST OF ABBREVIATION	xiv
LIST OF SYMBOLS	xv
ABSTRAK	xvi
ABSTRACT	xvii
CHAPTER 1 INTRODUCTION	1
1.1 Background	1
1.2 Heavy Metal in Wastewater	1
1.3 Toxicity of Cr Metal Ions.....	3
1.4 Nanostructured Materials	4
1.5 Photocatalytic Material	4
1.6 Waste Electronic and Electrical Equipment (WEEE).....	5
1.7 Problem Statement	7
1.8 Research Objectives	9
1.9 Scope of Work	9
1.10 Thesis Outline	10
CHAPTER 2 LITERATURE REVIEW	12
2.1 Introduction	12
2.2 Photocatalysis for Removal of Cr(VI)	12
2.3 1-D Metal Oxide Semiconductor	15
2.4 Properties of CuO.....	15

2.5	Synthesis Methods of CuO Nanostructure.....	16
2.5.1	Electrochemical Process	17
2.5.2	Chemical Precipitation.....	19
2.5.3	Hydrothermal	20
2.5.4	Electrospinning	21
2.5.5	Thermal Oxidation	23
2.6	Mechanism of Nanowires Formation.....	29
2.6.1	Vapor Liquid Solid (VLS) and Vapor Solid (VS)	29
2.6.2	Stress-induced Diffusion.....	32
2.7	Recovery Process of Valuable Metals from PCBs.....	34
2.7.1	Mechanical Process.....	35
2.7.2	Pyrometallurgical Process.....	36
2.7.3	Hydrometallurgical Process	37
CHAPTER 3 MATERIALS & METHODOLOGY		39
3.1	Introduction.....	39
3.2	Materials.....	40
3.3	Methodology	41
3.3.1	Recovery of Cu from WPCB	41
3.3.1(a)	Mechanical Processing of WPCB	42
3.3.1(b)	Removal of Organic Materials	45
3.3.1(c)	Separation of Magnetic Materials	46
3.3.1(d)	Leaching of WPCB powder	46
3.3.1(e)	Electrodeposition of Cu on Ti foil.....	47
3.3.2	Surface Preparation of Cu	49
3.3.3	Synthesis of CuO NWs via Thermal Oxidation.....	50
3.3.3(a)	Effect of Surface Roughness	51
3.3.3(b)	Effect of Oxidation Temperature	52

3.3.3(c)	Effect of Oxidation Duration.....	52
3.3.4	Photocatalyst Process.....	53
3.3.4(a)	Preparation of Synthetic Cr Stock Solution	54
3.3.4(b)	Photocatalysis Experiment	54
3.4	Characterization Techniques.....	55
3.4.1	Inductively Coupled Plasma Mass Spectrometry (ICP-MS)	55
3.4.2	Field Emission Scanning Electron Microscopy (FESEM)	56
3.4.3	X-Ray Diffraction (XRD).....	58
3.4.4	High Resolution Transmission Electron Microscopy (HRTEM) ..	59
3.4.5	Ultraviolet-Visible (UV-Vis) Spectrophotometry	60
CHAPTER 4	RESULTS AND DISCUSSION	61
4.1	Introduction.....	61
4.2	Electrodeposition of Cu Film on Ti Foil.....	61
4.3	Structural Observation of CuO NWs Formation by Thermal Oxidation	66
4.3.1	Effect of Surface Roughness.....	67
4.3.2	Effect of Thermal Oxidation Temperature	75
4.3.3	Effect of Thermal Oxidation Duration.....	82
4.4	Photocatalytic Experiment	87
CHAPTER 5	CONCLUSION AND RECOMMENDATION	98
5.1	Conclusion	98
5.2	Recommendations for future research	99
REFERENCES.....		100
APPENDIX.....		107

LIST OF TABLES

Table 2.1	Literature surveys on the fabrication of CuO NWs by thermal oxidation.	27
Table 3.1	List of the materials used throughout the experiment.....	40
Table 3.2	Electrodeposition parameter at various electrodeposition voltage. ...	48
Table 3.3	Electrodeposition parameter at various electrodeposition duration...	48
Table 3.4	Synthesis parameter of CuO NWs with different surface conditions of Cu foil.	51
Table 3.5	Synthesis parameter of CuO NWs in various oxidation temperature.	52
Table 3.6	Synthesis parameter of CuO NWs in various oxidation duration.....	53
Table 3.7	ICDD Card No. and the respective mineral name.	59
Table 4.1	Reduction percentage of Cr(VI) with CuO NWs grown under different oxidation parameters.	97

LIST OF FIGURES

Figure 1.1	Schematic diagram for mechanism of light activation of CuO.	5
Figure 1.2	Layers and component of WPCBs (Kaya, 2019).....	7
Figure 1.3	Flow of work involved and objectives to be achieved.....	11
Figure 2.1	Crystal structure of CuO. (Large atoms represent Cu atoms, small atoms represent O atoms)(Döring et al., 2004).....	16
Figure 2.2	FESEM images of (a) Anodized Cu foil with Cu(OH) ₂ nanoneedles; (b) Cu ₂ O NWs; (c) CuO/ Cu ₂ O nanoflake/NWs heterostructure (John & Roy, 2020).	18
Figure 2.3	FESEM images of CuO films at (a) 1.0 V; (b) 1.5 V; (c) 2.0 V; (d) 2.5 V (Wang et al., 2015).....	18
Figure 2.4	FESEM images of (a) CuO NWs; (b) AC/CuO NWs nanocomposite; (c) Agglomerated NWs (Lakkaboyana et al., 2019).	19
Figure 2.5	SEM image of CuO with irregular plate shape (Sirirak et al., 2022).	19
Figure 2.6	(a) Magnified SEM image showing CuO NWs; (b) HRTEM image of CuO NW (Cao et al., 2021).	20
Figure 2.7	FESEM image of CuO nanorods (Cai et al., 2021).	21
Figure 2.8	FESEM images of as-spun PVA-copper acetate composite fibers (top panel) and sintered CuO NWs (bottom panel) at low (left) and high (right) magnification (Vidhyadharan et al., 2014).	22
Figure 2.9	SEM images of precursor nanofibers (a) 6 wt% PVA; (b) 8 wt% PVA; (c) 10 wt% PVA (Cai et al., 2015).....	22
Figure 2.10	Cross-sectional view of an oxide layer (grown at 400 °C) showing the two oxide layers and the NWs (Goñalves et al., 2009).....	23
Figure 2.11	SEM images of CuO NWs by directly heating of Cu foils in air at (A) 300, (B) 400, (C) 500, (D) 600, (E) 700, (F) 800°C for 2h (Liang et al., 2010a).	24

Figure 2.12	Oxidized samples at 340 °C for 3, 20, 40 and 60 minutes (Moise et al., 2021).	25
Figure 2.13	SEM images of Cu substrates. A, D: surface without being sandblasted; B,E: surface sandblasted for 3 s; C, F: surface sandblasted for 9 s (Yuan & Zhou, 2012).	26
Figure 2.14	Schematic illustration of vapor liquid solid (VLS) growth mechanism (Musselman & Schmidt-Mende, 2011).	30
Figure 2.15	Foreign droplets at the top of n-type Si NWs grown on Si substrate (Musselman & Schmidt-Mende, 2011).	30
Figure 2.16	FESEM cross section image of Cu/ITO after deposition of Cu film (Nguyen et al., 2016).	31
Figure 2.17	FESEM cross section images of NWs grown at (a) 350 °C, (b) 400 °C, (c) 450 °C and (d) 500 °C for 5 hours (Nguyen et al., 2016).	31
Figure 2.18	Illustration of the stress induced diffusion for CuO NWs growth (Chen et al., 2012).	34
Figure 2.19	Flow diagram of metal recovery from e-waste (Rao et al., 2020).	35
Figure 2.20	Schematic diagram of centrifugal separation apparatus (Meng et al., 2018).	36
Figure 3.1	General overview of the research work.	39
Figure 3.2	Flowchart of the extraction of Cu from WPCB.	42
Figure 3.3	Condition of the motherboard before dismantling (left) and after dismantling (right).	43
Figure 3.4	Workflow of mechanical processing of WPCB.	44
Figure 3.5	Mozley gravity separator.	45
Figure 3.6	(a) Low SG particles moving down the slope, (b) Metallic materials (left) and organic materials (right).	46
Figure 3.7	Eriez rare earth magnetic roll separator.	46
Figure 3.8	Illustration of leaching setup (left) and solid liquid separation (right).	47
Figure 3.9	Illustration of the setup for electrodeposition.	48

Figure 3.10	Actual electrodeposition setup.....	49
Figure 3.11	Adhesion tape test for adherence quality of electrodeposited layer on Ti substrate.....	49
Figure 3.12	Flowchart for the formation of CuO NWs by thermal oxidation of Cu layer on Ti.....	50
Figure 3.13	Heating profile for the formation of CuO NWs on Cu electrodeposited Ti foil.	51
Figure 3.14	Flowchart for catalytic experiment.	53
Figure 3.15	Illustration of photocatalytic experiment.	55
Figure 3.16	ICP-MS (Perkin Elmer ICPMS Nexion 300).	56
Figure 3.17	(a) FESEM (FEI VERIOS 460L, 5 kV at Science and Engineering Research Center (SERC)), (b) FESEM (Hitachi Regulus 8220, 5 kV at Centre for Global Archaeological Research) and (c) SEM (Quanta FEG 450, 10 kV at School of Chemical Engineering).	58
Figure 3.18	HRTEM (TECNAI G2 20 S-TWIN, FEI).	60
Figure 4.1	Physical appearance of as electrodeposited layer at (a) 10 V, (b) 5 V and (c) 3 V for 60 minutes.	63
Figure 4.2	Physical appearance of as electrodeposited Cu layer for (a) 15 min, (b) 30 min, (c) 45 min and (d) 60 min at 2 V.	64
Figure 4.3	Physical appearance of the electrodeposited layer at 3 V (a) before and (b) after adhesive tape testing.	64
Figure 4.4	Optical microscope images of the deposited Cu layer at (a) Corner, (b) Middle, (c) End, (d) Ti/Cu intersection.....	65
Figure 4.5	XRD diffraction patterns for as electrodeposited Cu film on Ti foil.	66
Figure 4.6	Optical microscope and SEM images of the Cu layer with magnification of 10X and 1.2 kX respectively (a) and (b) 1200 grit; (c) and (d) 600 grit; (e) and (f) 400 grit.	68

Figure 4.7	Physical appearance of the Cu layer grinded with (a) 1200 grit, (b) 600 grit, (c) 400 grit SiC paper after being oxidised at 350 °C for 180 mins.....	68
Figure 4.8	FESEM cross section images (20 kX) of oxide layer formed on Cu layer ground with the (a) 1200 grit and (b) 400 grit SiC paper.	69
Figure 4.9	FESEM cross section images (40 kX) of oxide layer formed on Cu layer grinded with the (a) 1200 grit and (b) 400 grit SiC paper.	70
Figure 4.10	SEM images (20 kX) of the surface of oxidised Cu layer grinded with the (a) 1200 grit and (b) 400 grit SiC paper.....	70
Figure 4.11	EDX spectra of the three layers: (a) CuO NWs, (b) CuO layer, (c) Cu ₂ O layer and (d) locations where EDX analysis were performed.	72
Figure 4.12	Three-layered oxide formed after thermal oxidation at 350 °C for 3 hours.....	73
Figure 4.13	XRD diffraction patterns for (a) as electrodeposited Cu film before thermal oxidation, (b) Cu layer ground with the 1200 grit SiC paper after oxidation and (c) Cu layer ground with 400 grit SiC paper after oxidation.	75
Figure 4.14	Physical appearance of Cu layer oxidised at (a) 500 °C, (b) 400 °C, (c) 350 °C and (d) 300 °C for 180 mins.	76
Figure 4.15	Physical appearance of the Cu layer oxidized at 500 °C for 180 mins.	77
Figure 4.16	Optical microscope images (a) blisters, (b) delamination of the CuO layer from the Ti foil at 10X magnification.....	78
Figure 4.17	FESEM cross section images (20 kX) of Cu layer oxidized at (a) 500 °C (b) 400 °C, (c) 350 °C and (d) 300 °C for 180 mins.	79
Figure 4.18	FESEM cross section images (40 kX) of Cu layer oxidized at (a) 500 °C (b) 400 °C, (c) 350 °C and (d) 300 °C for 180 mins.	80
Figure 4.19	SEM images (40 kX) of the surface of Cu layer oxidised at (a) 500 °C, (b) 400 °C, (c) 350 °C and (d) 300 °C for 180 minutes.	81

Figure 4.20	XRD diffraction patterns for (a) as electrodeposited Cu film before thermal oxidation, (b) Cu layer oxidised at 500 °C and (c) Cu layer oxidised at 300 °C for 180 minutes.....	82
Figure 4.21	Physical appearance of the Cu layer oxidised for (a) 120 mins, (b) 60 mins, (c) 45 mins and (d) 30 mins at 400 °C	83
Figure 4.22	FESEM cross section images of Cu layer oxidised at 400 °C for (a) 180 min (same image as in Figure 4.18) (b) 120 min and (c) 30 mins at magnification of 10 kX and 20 kX.	84
Figure 4.23	SEM images of the surface of Cu layer oxidised at 400 °C for (a) 120 min and (b) 30 min.....	84
Figure 4.24	XRD diffraction patterns for (a) as electrodeposited Cu film before thermal oxidation, (b) Cu layer oxidised for 120 mins and (c) Cu layer oxidised for 30 mins at 400 °C.....	85
Figure 4.25	(a), (b), (d) HRTEM images and (c) FFT image of CuO NWs. (The NWs were produced by oxidation at 400 °C for 30 minutes.	86
Figure 4.26	Absolute conduction band and valence band energy levels of CuO and Cu ₂ O with respect to normal hydrogen electrode (NHE). Data taken from (Paquin et al., 2015).	87
Figure 4.27	Absorbance spectra of Cr(VI) in solution with presence of Cu layer grinded with (a) 1200 grit, (b) 600 grit and (c) 400 grit SiC paper after oxidation.	90
Figure 4.28	Photoreduction of Cr(VI) solution in the presence of Cu layer ground with 1200 grit, 600 grit and 400 grit SiC paper after oxidation.....	91
Figure 4.29	Absorbance spectra of Cr(VI) in solution with presence of Cu layer oxidized at (a) 500 °C, (b) 400 °C and (c) 300 °C for 180 mins.	93
Figure 4.30	Photoreduction of Cr(VI) solution in the presence of Cu layer oxidized at 500 °C, 400 °C and 300 °C for 180 mins.....	93
Figure 4.31	Absorbance spectra of Cr(VI) in solution with presence of Cu layer oxidized at 400 °C (a) 30 min, (b) 45 min, (c) 60 min and (d) 120 min.	96

Figure 4.32 Photoreduction of Cr(VI) solution in the presence of Cu layer oxidized at 400 °C for 30, 45 , 60 and 120 min. 96

LIST OF ABBREVIATION

A.u	Arbitrary Unit
CB	Conduction Band
Cr(III)	Chromium (III)
Cr(VI)	Chromium (VI)
d	Lattice Spacing
DI	Deionized Water
EDTA	Ethylene Diamine Tetraacetic Acid
EDX	Energy Dispersive X-Ray
FESEM	Field Emission Scanning Electron Microscopy
HRTEM	High Resolution Transmission Electron Microscopy
ICP-MS	Inductively Coupled Plasma Mass Spectrometry
ISO	International Organization for Standardization
NWs	Nanowires
pH	Hydrogen Potential
UV-Vis	Ultraviolet-Visible
VB	Valence Band
WEEE	Waste Electric and Electronic Equipment
WPCB	Waste Printed Circuit Board
XRD	X-Ray Diffraction

LIST OF SYMBOLS

E_g	Band gap energy
θ	Bragg angle
$^\circ$	Degree
$^\circ\text{C}$	Degree celcius
$^\circ\text{C}/\text{min}$	Degree celsius per minute
2θ	Diffraction angle
e^-	Electron
h^+	Hole
$\bullet\text{OH}$	Hydroxyl radical
$\%$	Percentage
$h\nu$	Photon energy
λ	Wavelength

SURFACE OXIDATION OF CU EXTRACTED FROM ELECTRONIC WASTE FOR CUO NANOWIRES FORMATION AND THEIR USE TO REDUCE CR(VI)

ABSTRAK

Cr(VI) dianggap sebagai logam berat toksik dan akan menjejaskan kesihatan mereka yang mengambilnya. Ia boleh memasuki ekosistem daripada air kumbahan pelbagai bidang. Dalam kajian ini, keupayaan dawai nano CuO untuk pengurangan Cr(VI) kepada Cr(III) telah disiasat. Cu mula-mula diekstrak daripada papan litar bercetak buangan dengan larut lesap dan elektrodeposisi lapisan Cu pada kerajang Ti. Kepekatan Cu terdapat dalam larutan larut lesap dan tercerna telah dicirikan menggunakan ICP-MS. Dawai nano CuO telah dibuat dengan mengoksidakan haba lapisan Cu terdeposit pada suhu antara 300 hingga 500 °C. Semua sampel telah diuji untuk pengurangan foto di bawah cahaya matahari selama 90 minit. Dawai nano CuO dicirikan menggunakan FESEM dengan EDX, XRD dan HRTEM. Parameter pengoksidaan yang disiasat ialah kekasaran permukaan, suhu pengoksidaan dan tempoh pengoksidaan. Pengoksidaan pada 350 °C telah dijalankan untuk menyiasat pertumbuhan dawai nano pada kekasaran permukaan lapisan Cu yang berbeza. Ketumpatan dawai nano yang tumbuh pada permukaan paling kasar adalah tidak seragam dengan purata panjang dan diameter 1015.3 dan 34.2 nm, justeru menghasilkan pengurangan paling sedikit Cr(VI) iaitu 44 %. Untuk kesan suhu, dawai nano terbentuk pada julat suhu 300 – 500 °C mempunyai panjang dan diameter antara 1798.31 - 539.5 nm dan 53.66 – 20.9 nm. Pengurangan 47.5 % dicapai pada sample teroksida pada 500 °C. Pelbagai tempoh pengoksidaan dikaji pada 400 °C antara 30 hingga 120 minit. Dengan tempoh pengoksidaan yang berpanjangan, panjang dan diameter dawai nano meningkat. Pengurangan 35 % dicapai untuk sampel teroksida selama 120 minit.

SURFACE OXIDATION OF CU EXTRACTED FROM ELECTRONIC WASTE FOR CUO NANOWIRES FORMATION AND THEIR USE TO REDUCE CR(VI)

ABSTRACT

Cr(VI) is considered a toxic heavy metal and will affect the health of those who consumed it. It can enter the ecosystem from various fields' wastewater. In this study, the capability of CuO NWs for the reduction of Cr(VI) to Cr(III) was investigated. The Cu was firstly extracted from WPCB by leaching and electrodeposition of the Cu layer on Ti foil. The concentration of Cu present in leaching and digested solution were characterized using ICP-MS. The CuO NWs were fabricated by thermal oxidizing the electrodeposited Cu layer at temperature between 300 to 500 °C. All samples were tested for photoreduction under sunlight for 90 minutes. The CuO NWs were characterized using FESEM with EDX, XRD and HRTEM. The oxidation parameters investigated were surface roughness, oxidation temperature and oxidation duration. Oxidation at 350 °C was conducted to investigate the growth of NWs on different surface roughness of Cu layer. The density of the NWs grown on the roughest surface was non-uniform with average length and diameter of 1015.3 nm and 34.2 nm, hence resulting in the least reduction of Cr(VI) which was 44 %. For the effect of temperature, the NWs formed at the temperature range of 300 – 500 °C had length and diameter between 1798.31 – 539.5 nm and 53.66 – 20.9 nm. 47.5 % Cr(VI) reduction was achieved for sample oxidized at 500 °C. Various oxidation duration was studied at 400 °C ranging from 30 to 120 minutes. With prolonged oxidation duration, the length and diameter of NWs formed increased. 35 % Cr(VI) reduction was achieved for sample oxidised for 120 minutes.

CHAPTER 1

INTRODUCTION

1.1 Background

For the past decade, semiconducting metal oxide nanomaterials have garnered the attention of researchers and intensive scientific work has been done to explore the possible applications in various fields. This is due to their exceptional physical and chemical properties such as having large surface area, high adsorption ability, high catalytic activity and high surface reactivity. Copper oxide (CuO) is an example of a semiconductor oxide. It can be synthesized by oxidising metallic copper, Cu. Nevertheless, as opposed to the use commercially available Cu, the metal was extracted from e-waste considering the vast amount of e-waste in the world these days and the scarcity of mineral resources.

Cu was first extracted from Waste Printed Circuit Board (WPCB) powder through leaching and was electroplated on a titanium (Ti) foil. The electroplated Cu was then thermally oxidised to form CuO nanowires (NWs). The synthesized CuO NWs were then used as photocatalyst for the reduction of hexavalent chromium (Cr(VI)) to trivalent chromium (Cr(III)) in water under natural sunlight (UV/visible light).

1.2 Heavy Metal in Wastewater

Water is a very important source which holds the key to survival of all living organisms on Earth. Even though water coverage on Earth is almost 70 %, however only 2.5 % of it is indicated as clean water which is available and safe for human consumption (Yahya et al., 2018). This amount of water is used for various human activities and after that, is treated and recycled so that it can be reused. Over the last decade, due to massive global human population and rapid industrialization, there has been a tremendous increase

in the demand for clean water supply. This water shortage situation might advance into a worldwide water predicament. With the growth of human activities and industries such as mining, agriculture, electroplating industry and metal smelting, the amount of water usage escalates and consequently generating similar amount of wastewater (Qasem et al., 2021).

Wastewater can be defined as a mixture of liquid that contains contaminants such as microorganisms, organic and inorganic materials and heavy metals, which are discharged from residential area, industrial or commercial premises (Naseem & Durrani, 2021; Qasem et al., 2021). The contamination level in the wastewater is alerting as it strongly affects human as well as brings serious consequences to the ecosystem. Amongst all the contaminants mentioned before, one of the main classes that is studied is heavy metal. Heavy metals have a relatively high densities which are usually greater than 5 g/cm³. Some of the most common heavy metals present in wastewater are mercury (Hg), lead (Pb), nickel (Ni), cadmium (Cd), arsenic (As), chromium (Cr) and etc. These carcinogenic heavy metals may accumulate in human bodies through the channel of food chain. In addition to direct health effects to human, heavy metals pollution can also lead to poisoning of animals and plants, reduction in crop yields, shortage of food sources, ecological imbalance and damage to biodiversity (Gao & Meng, 2021). Therefore, it is necessary to treat wastewater contaminated with heavy metals in the affected areas where wastewater management is usually absent or done poorly.

In the most recent Environmental Quality Report (EQR) by Department of Environment (DOE) of Malaysia in 2019, about 76.8 % of the water samples have shown that the concentrations of Fe were within Class II limit followed by Zn (99.9 %), Pb (98.7 %), As (98.9 %) and Cr (99.8%). This work focuses on Cr in the form of Cr(VI). Cr(VI) ions were removed by photocatalysis process on the CuO NWs synthesized from e-waste.

1.3 Toxicity of Cr Metal Ions

In heavy metal removal studies, Cr is among one of the most studied. It has been listed by the US Environmental Protection Agency (US EPA) as one of the priority pollutants. Cr is however a metal with various industrial and technological applications in the electroplating, textile, leather tanning, wood preservation and metallurgy field (Rosli et al., 2021). Cr's oxidation states vary from (II) to (VI) with the trivalent (Cr(III)) and hexavalent (Cr(VI)) being the two more stable ones (Tumolo et al., 2020). Cr(III) is a natural element which is mostly present in rocks, volcanic dust, plants, soil, animals and gases. It is less toxic and only affect plant, not humans. In fact, trace amount of Cr(III) is essential for human body health and is present in most foods and supplement. On the other hand, Cr(VI) is corrosive, toxic and carcinogenic. It occurs naturally due to erosion of Cr deposits but is more usually found as a result of industrial waste discharged such as wastewater. Inevitably, wastewater from industrial process contains large amounts of Cr(VI), and unless treated properly, Cr(VI) can enter surface water thus polluting the water (Sharma et al., 2022).

According to the recommendation from the World Health Organization (WHO), concentration of Cr(VI) in water should not exceed 0.05 mg/L which is also the maximum permitted value. The maximum permitted value of Cr(VI) is 0.05 mg/L as well. It is therefore crucial to remove Cr(VI) from the wastewater to prevent surface water concentrations exceeding this level. Cr(VI) can be removed by . Here, CuO in the form of NWs were fabricated as mentioned and used to remove Cr(VI) from stimulated wastewater.

1.4 Nanostructured Materials

NW is one class of nanomaterials. According to the ISO/TS 80004-1 document, nanomaterials (NMs) are described as material with length of 1 – 100 nm in at least one dimension and they exhibit dimension-dependent phenomena. They are classified in three groups namely 0-dimensional (0-D), 1-dimensional (1-D) and 2-dimensional (2-D). In this study, the nanomaterial produced was in a form of nanowire (NW) which is a 1-D nano-object. It has x and y dimensions in nanoscale but the long dimension in microscale (>100 nm) (International Organization for Standardization (ISO), 2015). NW is further defined as electrically conducting or semiconducting nanofiber. Properties of materials are size dependent in the nanoscale range. Within this size range, the quantum effect governs the material's properties and behaviour. As CuO is a semiconductor, the elongated structure can be considered as 1-D NW structure. NWs have high surface-to-volume ratio, high aspect ratio and high surface atoms. The high surface area provides numerous surface active sites, which yields excellent photocatalytic potential.

1.5 Photocatalytic Material

The metal oxide semiconductors that are commonly studied are n-type semiconductors such as TiO₂ and ZnO, which have electrons as the major charge carriers. The E_g of rutile and anatase TiO₂ are 3.0 eV and 3.2 eV respectively. For ZnO, the E_g is 3.37 eV (Sun et al., 2020). However, the wide bandgap n-type semiconductor can only perform well under UV radiation but not under visible light. According to Yu et al. (2015), for the solar energy, UV light only holds up to 4 % of the energy whereas the visible light accounts for 43 % of it. In practice, this has limited application of the n-type semiconductor photocatalyst in large scale. This is why many efforts have been made in order to improve photocatalytic performance of the n-type semiconductors upon visible

light irradiation. One of the methods is doping which reduces the width of the E_g as new energy levels are formed near the CB (Khlyustova et al., 2020). Not only that, the doping ions suppress the recombination of electrons and holes by introducing charge trapping sites (Li et al., 2020).

A small E_g has the tendency to enhance the photocatalytic properties of the photocatalyst as only a small amount of energy is required to generate electron-hole pair. CuO, which is a p-type semiconductor has a narrow E_g of 1.4 eV as shown in Figure 1.1. The majority charge carriers for p-type semiconductor are holes. The performance of CuO NWs for reduction of Cr(VI) to Cr(III) was investigated.

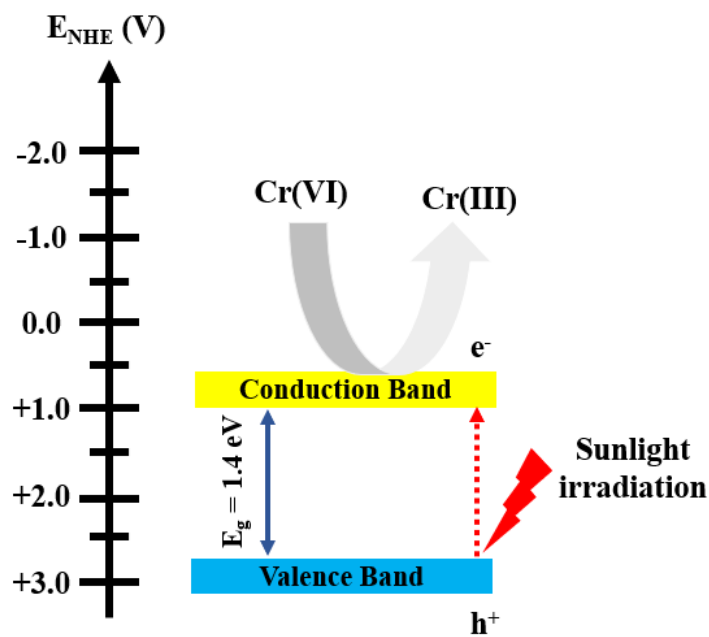


Figure 1.1 Schematic diagram for mechanism of light activation of CuO.

1.6 Waste Electronic and Electrical Equipment (WEEE)

The amount of waste electronic and electrical equipment (WEEE) or e-waste have been increasing rapidly in the last few decades as a result of technology innovations. Recent reports by the United Nations (UN), mentioned that in 2021, each person on this planet will generate 7.6 kg of e-waste, which will result in 57.4 million tonnes globally

(Murthy & Ramakrishna, 2022). Generally, WEEE contains high amount of heavy and precious metal such as gold (Au), silver (Ag), copper (Cu), iron (Fe), lead (Pb) and aluminium (Al), to name a few. Natural resources are diminishing at an alarming rate and the metals mined from the Earth's core are becoming scarce. In order to overcome metal scarcity, WEEE can be considered as secondary source by recovering those metals before the waste is disposed. Not only that, recovery of the metals from e-waste reduces the emission of carbon dioxide (CO₂) compared to virgin metal mining (Van Yken et al., 2021).

Among the WEEE there are, an average amount of WPCB takes up around 3 -5 % and is considered as one of the more valuable fraction of WEEE as it contains high concentration of base metal (Kaya, 2020). Generally, a PCB is made up of metallic and non-metallic materials which comprise of roughly 40 % metals, 30 % plastic components and 30 % ceramics. The base metals are mostly Cu, Fe, Al and Sn, precious metals like Au, Ag and Pd, and rare metals such as Pt, Ta, Ga and In (Burat & Özer, 2018). If these metals can be recovered, then they can be reused for other applications.

PCB is an electrical circuit board that electrically connects all the electronic components such as capacitors, resistors and insulators. The insulating board of the PCB is often made up of glass fiber or epoxy resin. On the surface of the board, there is a thin layer of Cu foil, which creates the conductive pathway of the circuit to connect the soldered electronic components on the PCB. A layer of solder mask will insulate the traces of the Cu (Rocchetti et al., 2018). The layers in PCB is shown in Figure 1.2. The use of PCB is very intensive as almost every electronic appliance around us contains PCB as the base. Example of the products are smartphones, laptops, games consoles, refrigerator, automotive components, medical devices and security system. As the demand of these products are now very high, the waste associated with them can be

expected to be very high as well. This work looks at the recovery of Cu from PCB which then will be converted to CuO: a semiconductor oxide. The semiconductor metal oxide, CuO is to be used as adsorbent and photocatalysts for removal of heavy metals from industrial wastewater.

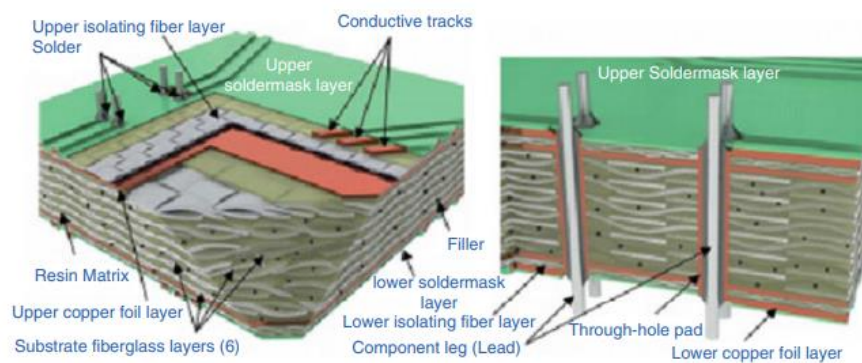
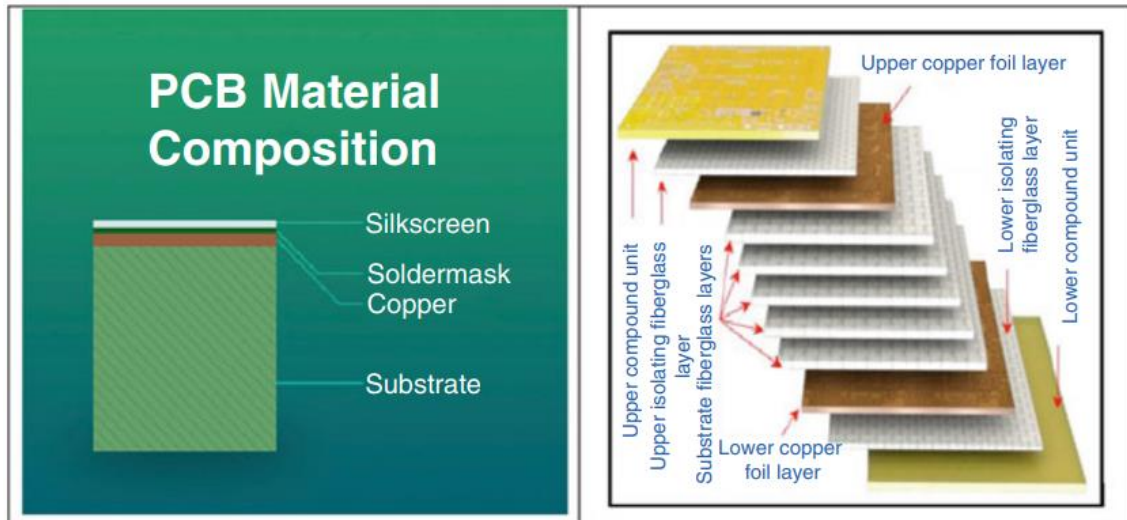


Figure 1.2 Layers and component of WPCBs (Kaya, 2019).

1.7 Problem Statement

The presence of heavy metals such as Cr especially Cr(VI) compounds in the wastewater has always caused environmental issue and an amount exceeding 0.05 mg/L as recommended by WHO might bring detrimental effect to human being. In this study, photocatalysis method is chosen as a technique to remove Cr(VI) as it offers easy treatment with no sludge production compared to the chemical-based separation method.

It is an ideal green energy technology for the purification for wastewater. Semiconductors are usually preferred to be used as photocatalysts due to their narrow band gap, particularly between 1.4 – 3.8 eV. Although TiO₂ dominates as reference photocatalyst, its relatively wider band gap (3.2 eV) becomes limitation for extended utility. The band gap of this material has limited the absorption of only small portion of the solar spectrum (UV region) (Ozawa et al., 2018). The larger bandgap would require higher energy to activate the photocatalyst. Thus, the search for non-TiO₂ based nanomaterials has become an active area of research in recent years. The use of narrower band gap material is desired and CuO is a narrow band gap semiconductor ($E_g = 1.4$ eV).

Synthesis of CuO NWs have been done in various methods such as hydrothermal, chemical precipitation, electrospinning and etc. However, these methods are time-consuming, expensive and complicated. In this work, CuO NWs are going to be synthesized via thermal oxidation of electrodeposited Cu recovered from WPCBs. Compared to those methods mentioned before, thermal oxidation is a straightforward and much simpler method. Many of the previous studies have managed to fabricate CuO NWs with a duration more than an hour. This research aims to fabricate CuO NWs at temperature of 350 °C which can be considered as low temperature process. The starting material will be Cu which will be produced from e-waste. Treatment of WPCB for Cu extraction was done and as no studies till date have reported using extracted Cu from e-waste for fabrication of CuO NWs, the work here is considered novel in this aspect. As to further reduce oxidation time/temperature, the effect of the surface roughness on the growth of CuO NWs was investigated in this study. The surface of the Cu foil was roughened with different grits of SiC paper to create different surface roughness. It is hypothesised that roughened surface can lead to faster growth and dense NWs can be formed at lower temperature.

CuO NWs are used as photocatalysts in the reduction of Cr(VI) into Cr(III). This provides other alternatives of using other metal oxides NWs to treat heavy metals in wastewater, instead of using TiO NWs which has been in the spotlight for a long time. Nonetheless, CuO is a well-known p-type semiconductor which has excess holes (holes are very oxidising but the process needed for Cr(VI) removal is reduction). The use of p-type material for reduction process requires further investigation such as exploring hole scavengers to capture holes (such as acetic acid) allowing for free electrons to be used to reduce Cr(VI) to Cr(III).

1.8 Research Objectives

The main focus of this research is to fabricate CuO NWs via thermal oxidation by inducing different degree of surface roughness, oxidation time and oxidation temperature.

The specific objectives are:

- i. To extract Cu from WPCB via leaching and electroplating to coat Cu layer on Ti foil.
- ii. To synthesize CuO NWs by thermal oxidation of the deposited Cu as in (i) by varying the surface roughness, oxidation duration and oxidation temperature.
- iii. To access the effectiveness of CuO NWs as a photocatalyst for reduction of Cr(VI) to Cr(III) under solar radiation.

1.9 Scope of Work

This work was divided into three parts which would be elaborated in detail in CHAPTER 3. For the first part, it involved mechanical processing, leaching and electroplating for extraction of Cu from WPCB in order to electrodeposit Cu on Ti foil. For the second part, the deposited Cu will be thermal oxidized to form CuO NWs. The Cu layer was ground with different grits of SiC paper to generate surfaces with roughness.

Surface morphology of the NW structures after thermal oxidation was observed and analysed using Field Emission Scanning Electron Microscope (FESEM) and High Resolution Transmission Electron Microscopy (HRTEM). For the phase identification, X-Ray Diffraction (XRD) was used. The photocatalytic reduction test was done by immersing the samples in synthetic Cr(VI) solution under sunlight. Ultraviolet-visible (UV-vis) spectrophotometer was used to measure the concentration of aqueous solution of Cr. The flow of work is summarised in Figure 1.3.

1.10 Thesis Outline

There are five chapters in this thesis. In CHAPTER 1, introduction, problem statement, objectives and the scope of work are discussed. CHAPTER 2 mentions about the different methods for extracting Cu from WPCB as well as the fabrication techniques of CuO nanostructure. Next, in CHAPTER 3, the materials, methodology and the characterization techniques used are discussed. Meanwhile, results and discussion are mentioned in CHAPTER 4. Last but not least, CHAPTER 5 concludes the work and recommendations for future work are discussed.

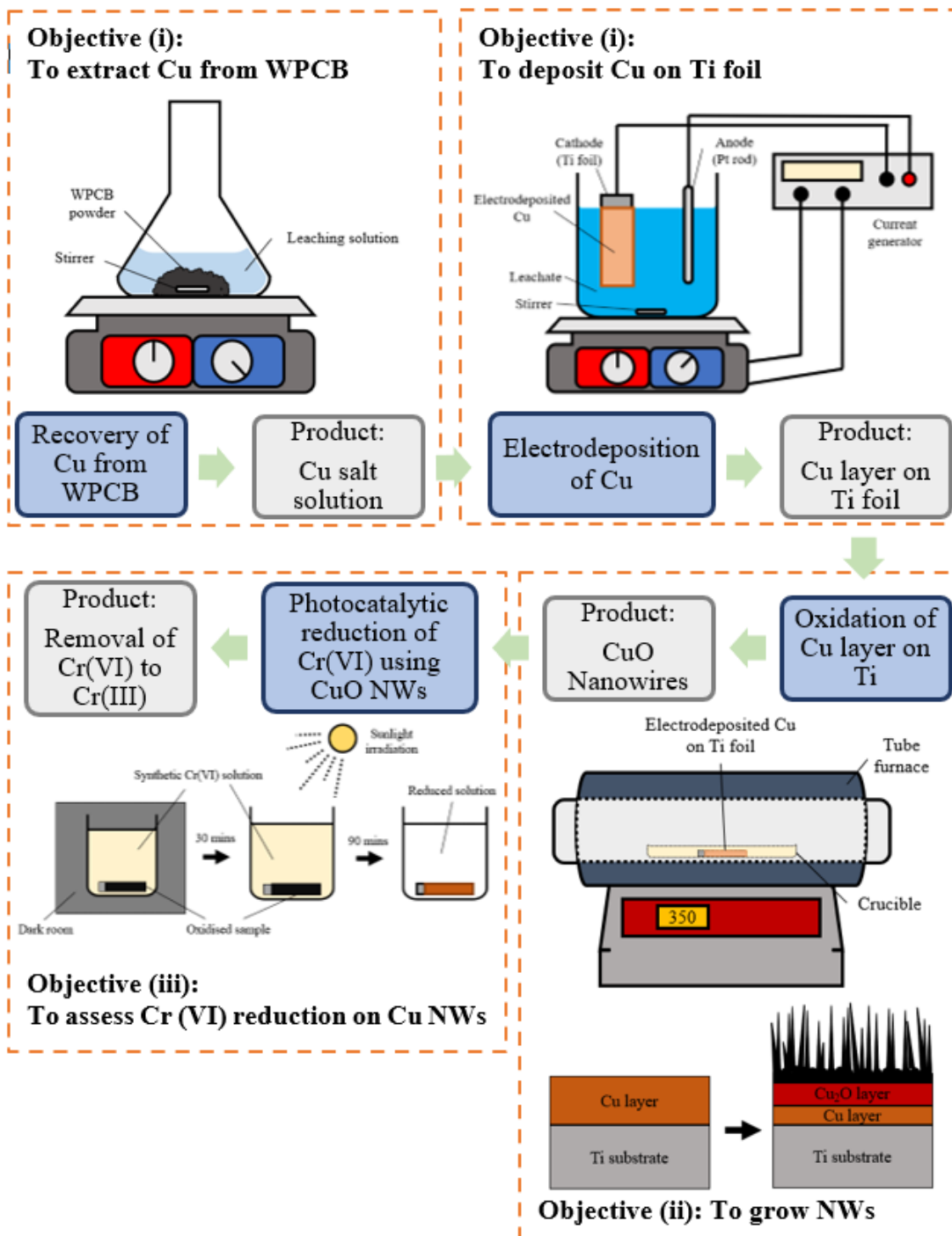


Figure 1.3 Flow of work involved and objectives to be achieved.

CHAPTER 2

LITERATURE REVIEW

2.1 Introduction

In this chapter, various recovery process of valuable metals from PCBs will be discussed. Next, the properties of 1-D metal oxide semiconductor as well as CuO NWs will be discussed. Besides that, different synthesis methods for the formation of CuO nanostructure are mentioned in this chapter.

2.2 Photocatalysis for Removal of Cr(VI)

There are numerous ways to achieve the removal of heavy metals such as adsorption, ion exchange, membrane filtration, chemical precipitation and photocatalysis (Deng et al., 2018). Among these treatment methods, photocatalytic technology has attracted attention of many researchers due to its high efficiency, strong redox ability, energy conservation and mild reaction condition (L. Wang et al., 2008; Zhang & Itoh, 2006). This technology uses non-toxic materials which replaces chemical compounds with appropriate wavelength of lights. It does not require energy input other than light energy. Therefore, this environmentally friendly feature is harmonious with the purpose of water treatment. At present, nanostructured photocatalytic materials which include metal oxides such as TiO₂, ZnO, Fe₂O₃, Cu_xO, SnO₂, etc. have been the focus of intense studies these past years. These metal oxides have semiconductor structures. In this study, the photocatalyst that is going to be studied is cupric oxide (CuO) which is a p-type semiconductor. When the semiconductor material is irradiated by light, electrons (e⁻) located in the valence band (VB) may jump to conduction band (CB) and may leave a positively charged hole (h⁺) on VB, provided that the energy of the photon of the incident light is greater than or equal to the band gap energy between VB and CB. This pair of e⁻

and h^+ will migrate to the surface of the semiconductor to undergo a series of oxidation and reduction reaction, which are embodied in the conversion of different valence states in the treatment of heavy metals (Ullah et al., 2021; Ulyankina et al., 2020; Wang et al., 2021).

Photocatalytic technology has dated way back at 1971, when Fujishima and Honda achieved a breakthrough for using a semiconductor electrode which is TiO_2 electrode irradiated under ultraviolet light for water splitting (Marschall, 2021). Compared to metals, there is no overlapping of the conduction band (CB) and the valence band (VB) in semiconductor. A bandgap exists between the CB and VB, allowing transition of electrons from VB to CB at low energy.

The occurrence of photocatalysis is based on the energy band theory (Sun et al., 2020). Under light irradiation, the metal oxide semiconductor photocatalyst is activated. When the semiconductor absorbs the photon that has energy equal to or more than the band gap (E_g), the electron transitions from VB to CB, generating hole behind at VB. This pair of electron and hole will migrate to the surface of the photocatalyst, initiating reaction with the particles adsorbed on the surface of the photocatalyst. Simultaneously, recombination of electron and hole occurs and this reaction releases heat that obstructs the quantum efficiency of the photocatalysis (Sun et al., 2020). Ideally, in order to improve the efficiency, increase in the rate of charge transfer is what we yearned for.

There is not much literature work studying the capability of solely CuO NWs as photocatalyst in the reduction of Cr(VI) to Cr(III). CuO nanostructure is normally used by researchers in order to form nanocomposite with another semiconductor material. In a recent study by Zhou et al. (2020), a p-n hetero-nanoforest structure was synthesized to be used as photocatalyst to reduce Cr(VI). The structure consisted of p-type CuO NWs as tree trunks and polar facet regulatory n-type ZnO nanodisk as tree leaves. The degradation

of Cr(VI) was carried out under a Xenon-lamp irradiation. It was reported that bare CuO NWs exhibited 40 % photodegradation of Cr(VI) in 30 minutes. As for the hetero-nanoforest structured sample, the heavy metals degraded totally within 20 minutes.

Aside from that, many researchers have fabricated CuO with other n-type metal oxide semiconductors such as TiO₂ to form heterostructured nanocomposite which is used in the reduction of Cr(VI) to Cr(III). Udayabhanu et al. (2020) had carried out photocatalytic reduction of toxic Cr(VI) under sunlight for four hours and 55 % of Cr(VI) was reduced. 10 mg of the photocatalyst was added into 100 mL of 1 mM potassium dichromate solution. The photocatalyst used was Cu-TiO₂/CuO nanoparticles. The doping of Cu into the TiO₂ lattice functioned to narrow down the wide bandgap of TiO₂ and to shift the absorption from the ultraviolet region to the visible region in the solar spectrum. The contact of the surface between CuO and Cu-TiO₂ composite created a p-n type semiconductor heterojunction, which separated the photo-induced electron hole pair as a result of internal electric field (Reddy et al., 2018).

Another study by Wang et al. (2020) combined CuO, TiO₂ and reduced graphene oxide (rGO) to synthesize TiO₂/rGO/CuO nanocomposites through hydrothermal method. CuO was in charge in separating the electron-hole pairs faster whereas the rGO framework allowed faster transfer of electrons. CuO in the form of nanoparticles and TiO₂ in the form of nanorods were grafted onto the rGO framework. The structure was used to photoreduction of Cr(VI). Complete photoreduction was achieved within 80 minutes of irradiation time.

Aside from that, Yu et al. (2015) developed a 3-D heterohierarchical device consisted of 2-D CuO nanosheets and 1-D ZnO nanorods. With the presence of the nanocomposite as the photocatalyst in 40 mL of 20 ppm Cr(VI) solution, it was reported

that complete degradation of Cr(VI) could be achieved within 80 minutes of irradiation under Xenon lamp.

2.3 1-D Metal Oxide Semiconductor

1-D nanostructures such as nanowires, nanorods, nanofiber, nanowhiskers and nanotubes have attracted much interest due to their extraordinary physical and chemical properties in nanoscale as compared to the properties when the material is in bulk form, particularly for 1-D metal oxide semiconductor. The thickness and the width of the 1-D nanomaterials are restricted in nanoscale, whereas the length can range from micrometer to millimeter long. When the metal oxide semiconductor is in nanoscale, the 1-D nanostructures possess high aspect ratio as well as large specific surface area. This means that a substantial portion of the atoms actively engage themselves for surface reactions. Owing to these abundant active sites on the surface, their catalytic behaviour and directional charge transport properties, these make the 1-D morphologies are very attractive.

2.4 Properties of CuO

The two types of copper oxides are cupric oxide (CuO) and cuprous oxide (Cu₂O). In this study, the photocatalyst that is going to be studied is cupric oxide (CuO). It is categorized into the transition metal oxide group with a monoclinic structure as shown in Figure 2.1. In this structure, Cu is coplanarly surrounded by four oxygen atoms sitting on the corners of a nearly rectangular parallelogram (Döring et al., 2004). CuO is a p-type semiconductor with a narrow band gap ($E_g = 1.4$ eV). It is due to this small band gap material which causes an extensive range of solar spectrum can be utilized to produce sufficient charge carriers. Thus, CuO photocatalyst shows strong absorption in the visible

spectrum when compared to nanostructured samples of other metal oxide semiconductor such as TiO₂ exhibiting absorption in the UV region.

Besides that, CuO also possesses other properties such as antimicrobial activity, photovoltaic properties, high chemical and thermal conductivity. It is also non-toxic and environmental friendly. Therefore, CuO has been popularly used for applications in gas sensors, superconductors, batteries, antimicrobial material and photovoltaic products (Nkhaili et al., 2020; Xiang et al., 2018).

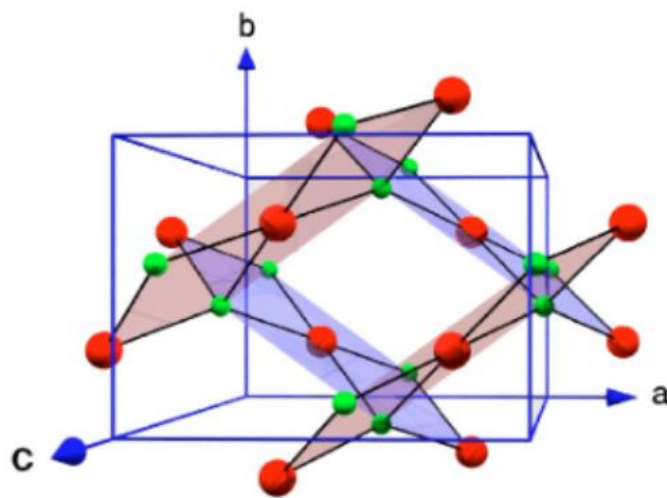


Figure 2.1 Crystal structure of CuO. (Large atoms represent Cu atoms, small atoms represent O atoms) (Döring et al., 2004).

2.5 Synthesis Methods of CuO Nanostructure

CuO has been synthesized in many different forms in nanoscale, which includes nanoparticles, nanofiber, nanoflakes and NWs. Due to the potential applications of nanostructured CuO in various field such as in gas and humidity sensor (Hsueh et al., 2011; Y. Li et al., 2008), glucose sensor (X. Liu et al., 2017), photovoltaics (Wang et al., 2011), field emission (Hsieh et al., 2003), field effect transistors (FETs) (Liao et al., 2009) and ion battery (H. Liu et al., 2015; Tan et al., 2016) various methods have been investigated in order to synthesize 1-D CuO NWs. Some of those methods include electrochemical process (John & Roy, 2020; Stepniowski & Misiolek, 2018), chemical

precipitation (Lakkaboyana et al., 2019; Sirirak et al., 2022), hydrothermal method (Y. Cai et al., 2021; J. Cao et al., 2021; Shrestha et al., 2010), electrospinning (Vidhyadharan et al., 2014) and thermal oxidation (Dey et al., 2022; Moise et al., 2021; Sondors et al., 2020).

2.5.1 Electrochemical Process

Anodization is an electrochemical process which often includes a potentiostat with a three-electrode system. John & Roy (2020) fabricated Cu₂O NWs by electrochemical anodizing Cu foil in KOH with constant current of 10 mA/cm² for a minute, followed by annealing at 450 °C for 2 hours. By further hydrothermal treating the samples in an autoclave containing KOH solution at 100 °C for different duration, CuO nanoflakes were synthesized over the surface of Cu₂O NWs as shown in Figure 2.2(c). Through the annealing process, the Cu(OH)₂ nanoneedles shown in Figure 2.2(a) transformed into Cu₂O NWs shown in Figure 2.2(b).

Another study by Wang et al. (2015) carried out the electrochemical synthesis in an undivided electrochemical cell. A Cu plate of 6 mm thickness was used. The electrolyte used contained 0.8 M of NaOH aqueous solution. Different anodized voltages were applied at 25 °C for 10 minutes. After 10 minutes, the Cu plate was taken out and heated for another 10 minutes at 300 °C, followed by cooling to room temperature. From Figure 2.3, it could be observed that there was absence of NWs when the voltage was at 1.0 V and 2.5 V. At 1.5 V, the CuO NWs formed had average diameter of 25 nm with average length of 5 μm. The NWs were interlaced with each other, forming a net structure. At 2.0 V, the NWs aggregated, forming short length bundles. Therefore, in order to fabricate NWs, the voltage shall not be too high or too low. A very low voltage was insufficient for the reaction to take place, whereas a very high voltage would cause the intermediates to precipitate.

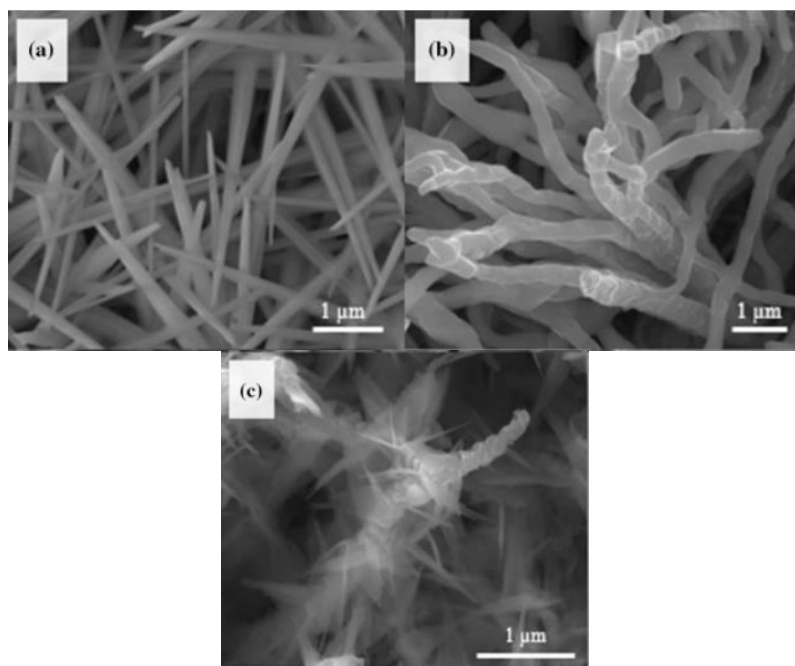


Figure 2.2 FESEM images of (a) Anodized Cu foil with $\text{Cu}(\text{OH})_2$ nanoneedles; (b) Cu_2O NWs; (c) $\text{CuO}/\text{Cu}_2\text{O}$ nanoflake/NWs heterostructure (John & Roy, 2020).

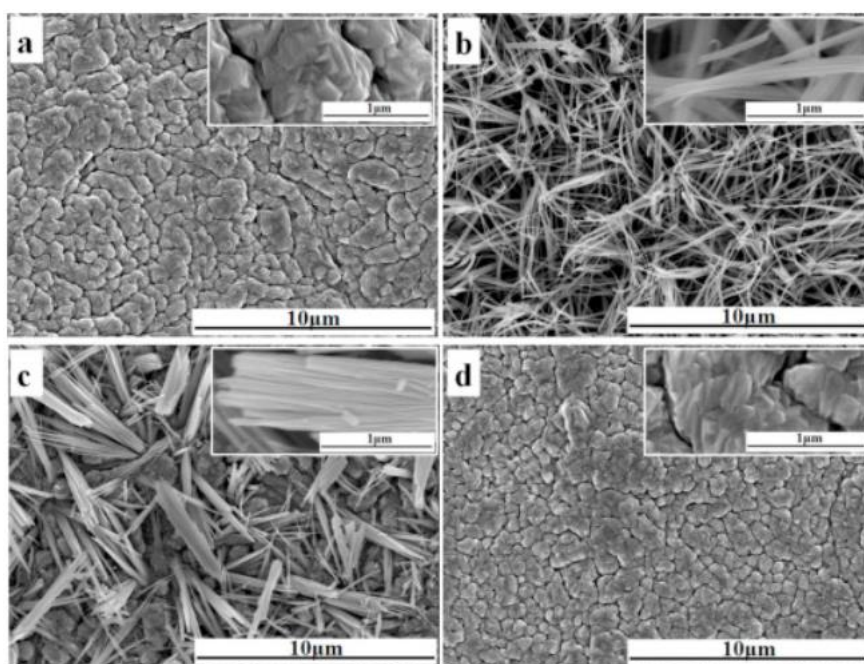


Figure 2.3 FESEM images of CuO films at (a) 1.0 V; (b) 1.5 V; (c) 2.0 V; (d) 2.5 V (Wang et al., 2015).

2.5.2 Chemical Precipitation

The chemical precipitation method is one of the low cost and effective processing route to grow nanostructured CuO. By governing the temperature, reaction duration, concentration and pH of the precursor, the morphology of the nanostructures can be controlled (Goswami et al., 2012). Lakkaboyana et al. (2019) carried out synthesis of CuO NWs on activated carbon through chemical precipitation for the removal of methylene blue from aqueous solution. From Figure 2.4 (a), the CuO NWs were seemed to be in the form of flowers due to surface regulation, oriented attachment and strong van der Waals attraction between the NWs. The average size of the NWs formed was between 15 to 17 nm. Similarly to Lakkaboyana et al. (2019), the CuO structure shown in Figure 2.5 as reported by Sirirak et al. (2022) showed similar condition as in Figure 2.4 (a). The irregular plate shape of CuO formed was reported having length of 1378 nm and width of 430 nm.

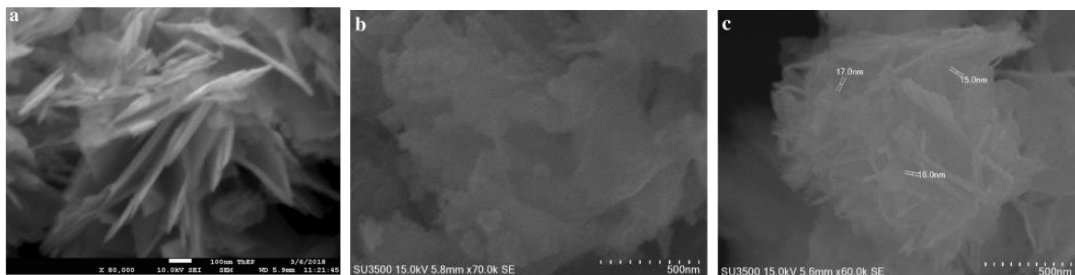


Figure 2.4 FESEM images of (a) CuO NWs; (b) AC/CuO NWs nanocomposite; (c) Agglomerated NWs (Lakkaboyana et al., 2019).

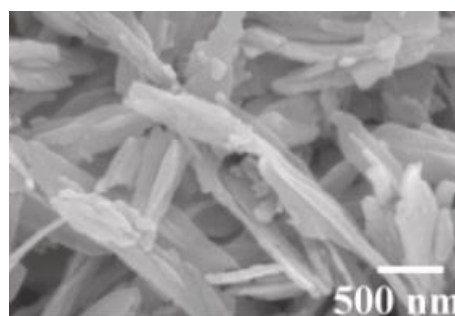


Figure 2.5 SEM image of CuO with irregular plate shape (Sirirak et al., 2022).

2.5.3 Hydrothermal

Another method which had been investigated to synthesize CuO NWs are hydrothermal method. A study by Cao et al. (2021) prepared Ag/CuO NW arrays with the combination of anodic aluminium oxide (AAO) template and hydrothermal reaction. The powder mixture of Ag and CuO was placed between the AAO template and the Pt foil. Then, it was heated in a furnace at 970 °C for 30 mins. After cooled down, the sample was transferred into an autoclave and heated in aqueous NaOH solution for an hour at 250 °C. During the hydrothermal process, Cu dissolved in the NaOH solution and formed CuO NWs. As shown in Figure 2.6, the SEM image on the left showed the surface was covered with NWs and the HRTEM image on the right indicated that the smooth NWs were CuO NWs. Another recent study by Cai et al. (2021) used this method to synthesize CuO nanorods. The precursor was put into an autoclave and heated at 160 – 180 °C for 4 hours. After drying, the sample was calcined at 600 °C for 3 hours. The synthesized CuO nanorods had an average diameter ranging from 30 to 50 nm as shown in Figure 2.7.

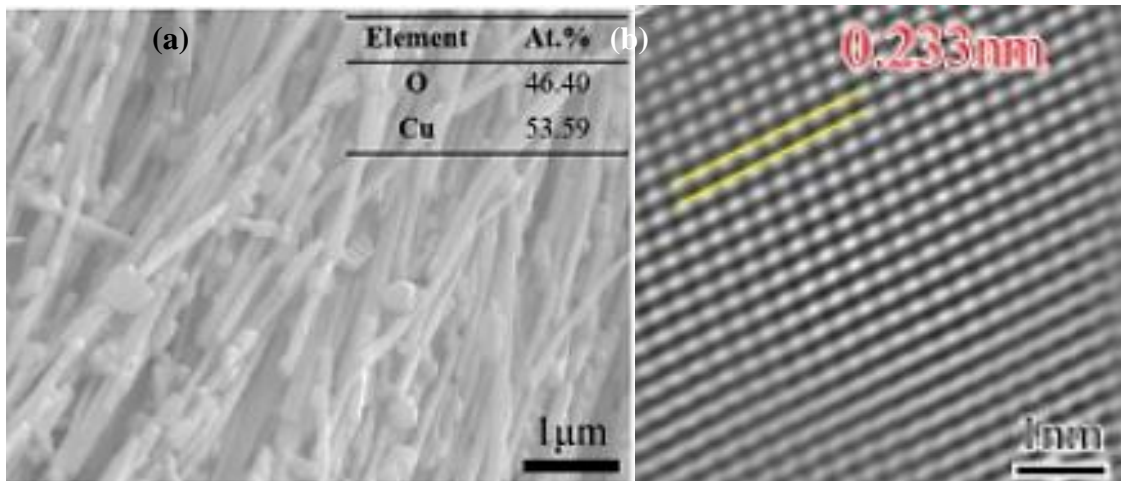


Figure 2.6 (a) Magnified SEM image showing CuO NWs; (b) HRTEM image of CuO NW (Cao et al., 2021).

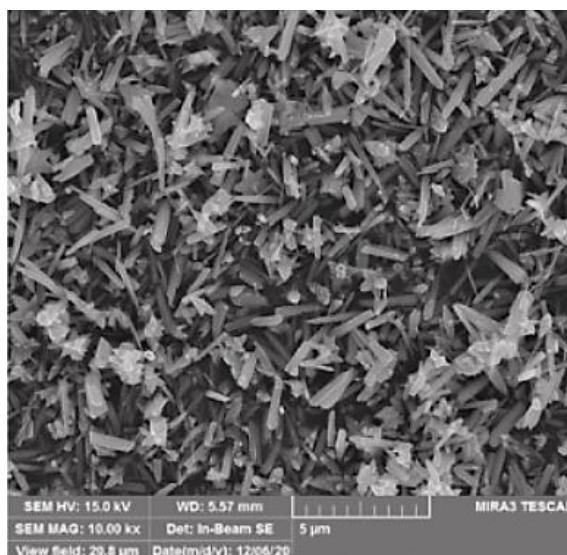


Figure 2.7 FESEM image of CuO nanorods (Cai et al., 2021).

2.5.4 Electrospinning

In this technique, a polymeric solution is charged and injected through a spinneret under the presence of an electric field to produce a continuous fiber on a collector surface. A study by Vidhyadharan et al. (2014) developed CuO NWs with diameter range of 30 – 50 nm using an aqueous polymeric solution-based electrospinning process. The solution was spun at 0.5 mL/h and at 24 kV. Then, the fibers were calcined at 500°C in air for 60 minutes. Figure 2.8 shows the FESEM images of as-spun and annealed NWs. It was observed that after annealing, the diameter of the wires decreased. The reported diameter for as-spun wires were around 210 nm and after annealing were reduced to ~30 – 50 nm. Besides that, Cai et al (2015) synthesized the CuO nanofibers through electrospinning as well using different solutions in order to study the effect of viscosity. From Figure 2.9, it was shown that some nodes were present among the electrospun nanofibers from 6 wt% PVA solution. As for the 8 wt%, the nanofibers were smooth, unlike the ones observed at 10 wt% which were stuck together. Another study by Sun et al. (2018) successfully prepared CuO NWs with diameter ranging from 130 – 275 nm with the flow rate and voltage set at 0.1 mm/min and 10 kV respectively. The as spun fibers were heated on a

hot plate for 15 minutes at 150 °C and subsequently calcined in the air for 2 hours at 500 °C.

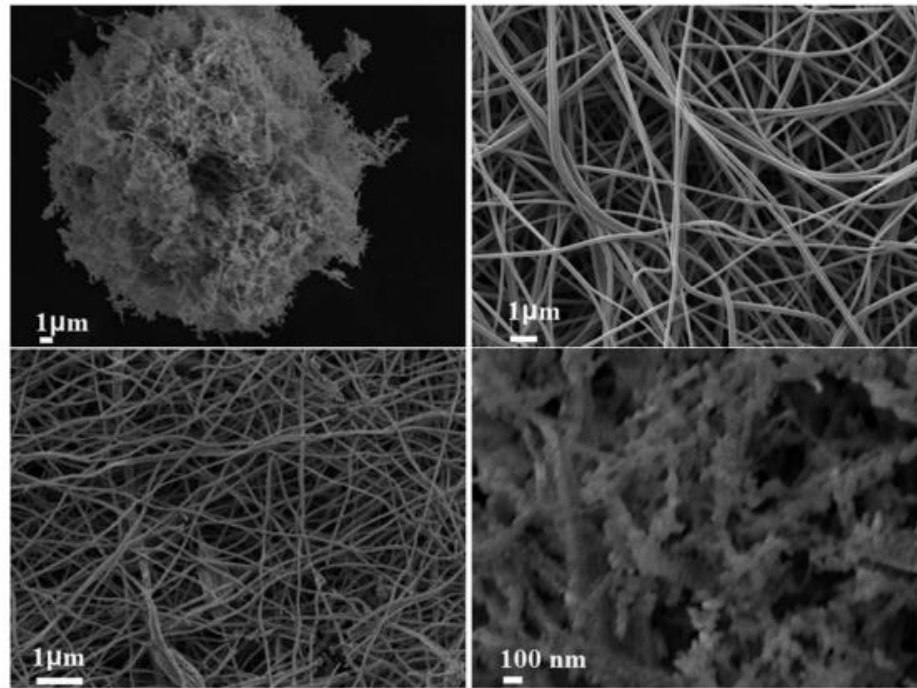


Figure 2.8 FESEM images of as-spun PVA-copper acetate composite fibers (top panel) and sintered CuO NWs (bottom panel) at low (left) and high (right) magnification (Vidhyadharan et al., 2014).

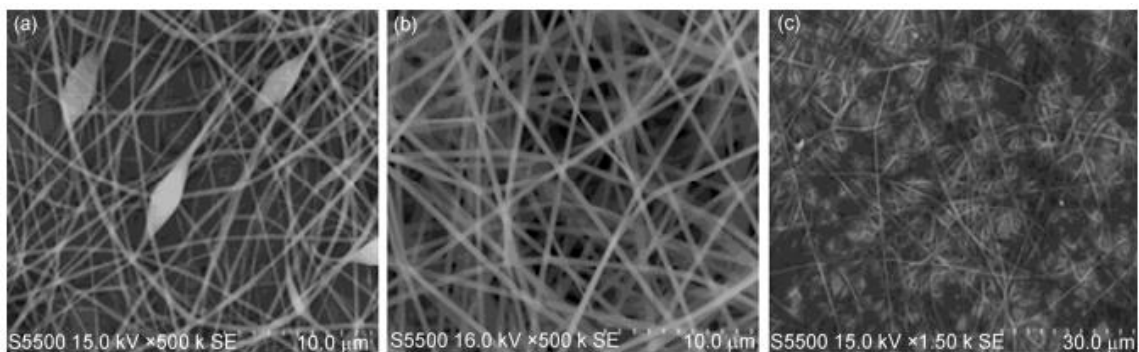


Figure 2.9 SEM images of precursor nanofibers (a) 6 wt% PVA; (b) 8 wt% PVA; (c) 10 wt% PVA (Cai et al., 2015).

2.5.5 Thermal Oxidation

Thermal oxidation method is considered as one of the simplest and economical method to synthesize CuO NWs. Direct oxidation of the Cu substrate such as foils, wires, sheets is the easiest method to produce large scale of CuO NWs. During this process, the Cu surface is oxidized and a Cu_2O layer is formed. This layer functions as a precursor of the formation of CuO NWs.

According to studies by Goñalves et al. (2009) and Hansen et al. (2011), the CuO NWs formation on the Cu surfaces involves a $\text{Cu}_2\text{O}/\text{CuO}$ double layer with cuprous oxide (Cu_2O) being the bottom layer and CuO on top of it. Figure 2.10 shows the cross-sectional view of an oxide layer (grown at 400 °C) showing two oxide layers and the NWs. For temperatures above 800 – 900 °C, mainly Cu_2O is formed at the oxide/air interface. As the temperature is lowered between 600 – 900 °C, grain boundary diffusion becomes relevant and a thin layer of CuO is formed over the Cu_2O layers. For temperatures below 500 °C, the grain boundary diffusion becomes dominant (Goñalves et al., 2009).

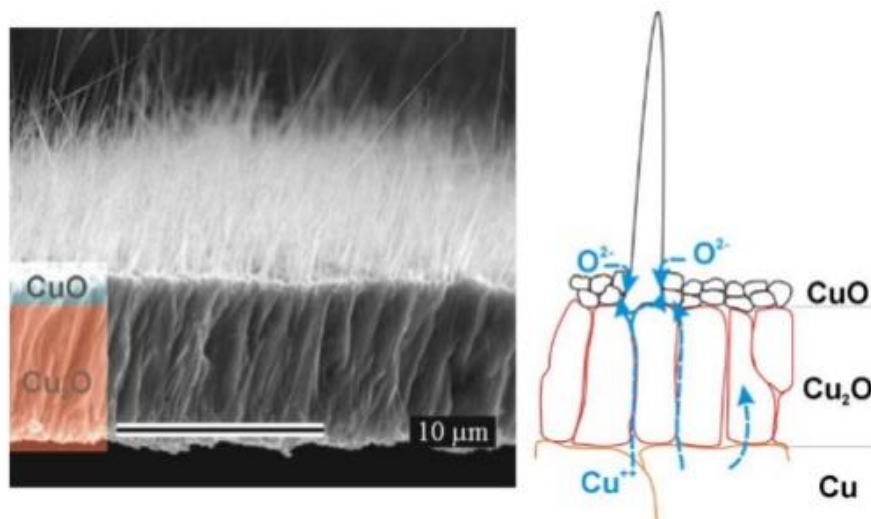


Figure 2.10 Cross-sectional view of an oxide layer (grown at 400 °C) showing the two oxide layers and the NWs (Goñalves et al., 2009).

Liang et al. (2010a) studied the growth of CuO NWs under different heating temperatures. From the morphology as seen in Figure 2.11, after oxidation at 300 °C, no NWs were observed. The NWs formed at 400 °C were very small and the orientation was not conformed, in fact, the NWs were curved. After heating at 500 °C, longer NWs were formed, with length ranging from 2 – 15 μm and diameter from 100 – 250 nm. The NWs formed at 600 °C were straighter than that formed at 500 °C. At 700 °C, the number of density of NWs observed decreased, while only a few of NWs were observed. At 800 °C, only large oxide grains were formed.

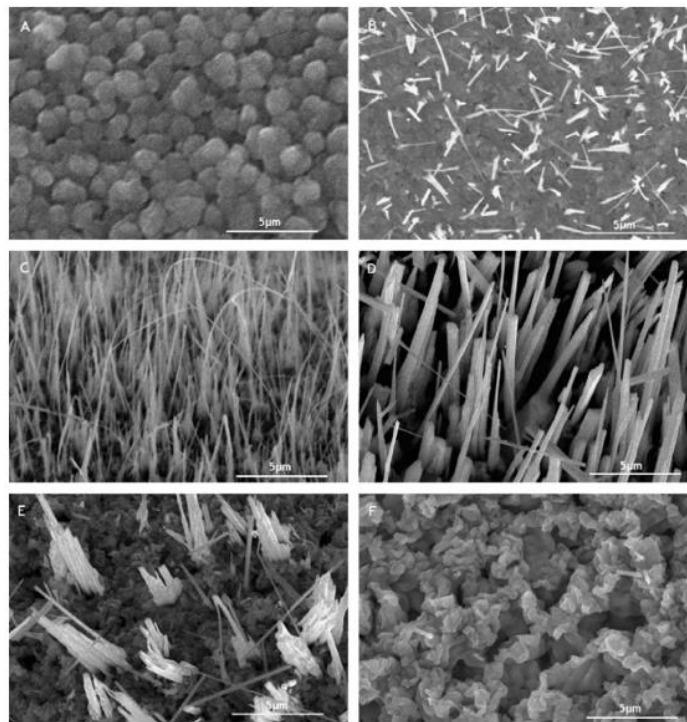


Figure 2.11 SEM images of CuO NWs by directly heating of Cu foils in air at (A) 300, (B) 400, (C) 500, (D) 600, (E) 700, (F) 800°C for 2h (Liang et al., 2010a).

In a very recent study by Moise et al. (2021), the CuO NWs were obtained by oxidizing poly-crystalline Cu foils at 320 °C and 340 °C in air under atmospheric pressure. The oxidizing duration was varied within one hour. From many of the previous studies as tabulated in Table 2.1, it is already known that formation of CuO NWs can usually be generated at the oxidation temperature ranging from 300 °C to 600 °C. Similarly to what